THE EFFECTS OF HEATING AND COOLING RATE ON THE CHARACTERISTICS OF THE CALORIMETRIC GLASS TRANSITION FOR GLASSY POLYMERS

JOHN R. SAFFELL *

Department of Metallurgy and Materials Science, University of Cambridge, Cambridge (Gt. Britain)

(Received 19 March 1979)

ABSTRACT

DSC was used to study the characteristic endotherm which occurs when reheating a glass back to the liquid state. Anionic polystyrene, PMMA, polycarbonate, and polysulfone were tested, varying both the cooling and reheating rates over two decades. In this initial paper on these results, an experimental technique optimized for glassy polymers is explained, and the proper method for correcting thermal lag is outlined. The variation of the onset, peak and fictive temperatures is shown for polystyrene and polysulfone. Results are also reported for the first time on the shift of the endothermal glass transition, measured while cooling.

INTRODUCTION

The effects of cooling rate, annealing time, and reheating rate on the glass transition endotherm have been studied for four glassy polymers. This initial paper from this work has a three-fold purpose: (1) to demonstrate an effective DSC technique for glassy polymers, (2) to show the proper method of thermal lag correction in low-conductivity glasses, and (3) to report the shifts of the characteristic temperatures of the glass transition endotherm as a function of both cooling and reheating rate.

EQUIPMENT AND MATERIALS CHARACTERIZATION

A DuPont 990 with DSC cell was used for the thermal analysis. Also, results obtained from a Perkin-Elmer DSC II are compared where relevant. The four polymers were: Pressure Chemicals anionic PS ($\bar{M}_n = 2 \times 10^5$, $\bar{M}_w/\bar{M}_n = 1.06$); ICI Perspex (PMMA) ($\bar{M}_w = 1.5 \times 10^7$, $\bar{M}_w/\bar{M}_n = 3.1$); Makrolon 3201 (PC, high viscosity extruded sheet); and injection moulded Union Carbide Udel (polysulfone).

---

* Present Address: Solomat S.A., Recherches sur les Matériaux, Avenue Division Leclerc, Ballainvilliers, France.

EXPERIMENTAL TECHNIQUE

Although the present DSC instruments are easy to operate, the problems of low thermal conductivity and shape changes make polymers difficult to study. A clear outline of the preferred experimental technique is therefore necessary. The solutions to some of these experimental problems are defined below.

The thermal conductivity of the flushing gas should be low, as shown by the problem of spurious peaks when helium is used [1]. Although surface radiation losses are a theoretical source of error, at temperatures less than 350°C radiation losses can be ignored, and pan lids, used to change surface emissivity, cause no noticeable change in the thermogram. In fact, a lid is a potential source of error due to stress generation during glass formation. The effect of pan location in the cell is important [1], and previous experience on the DuPont 990 shows that the distance from the sample center-of-mass to the thermocouple junction affects the thermal lag calibration. The sample weight should be kept small (less than 10 mg) to minimize thermal lag, to prevent peak broadening and to avoid sample—reference C_p mismatch [1].

The sample preparation technique is critical for repeatable thermograms; the initial run of the unmelted sample is the run which is most susceptible to spurious peaks arising from sample flow and stress relaxation. Since sample relaxation can alter the sample—pan contact, we have found that a thin coat of silicone oil on the sample before placing it in the pan is useful when testing un-premelted specimens prepared from the bulk (this DSC study was performed on pre-melted samples without silicone oil). If the sample—pan interface can be maintained, then differences between sample preparation techniques are negligible.

In order to measure T_g while cooling, a technique suitable for the DuPont 990 was developed. We tested only one sample of each polymer type, eliminating errors from changing sample mass and geometry: the samples were initially heated to $T_{l,l} + 20°C$ [2], then immediately cooled to room temperature at 10° min^{-1}. The flushing gas was argon (one half the thermal conductivity of nitrogen), and sample masses were between 2.3 and 6.4 mg; lids were not used. After much trial and error, we adopted the following method for sample cooling: the flushing gas was argon at 50 ml min^{-1}, but the rate was reduced to 25 ml min^{-1} for fast cools, which increased the signal-to-noise ratio of the cooling thermogram. Nitrogen was used as the cooling gas, at flow rates from 2 to 10 l min^{-1}; for fast cooling the nitrogen was passed through copper coils immersed in liquid nitrogen. This pre-cooling caused the nitrogen flow rate to fluctuate severely, which affected the ambient pressure on top of the cell, which in turn varied the argon flow rate. Therefore, a compressor working as an evacuator was attached to the vacuum inlet to remove the nitrogen after it passed through the cell block.

The quality of the thermogram is very sensitive to variations in the flushing gas flow rate, so a two-stage regulator, followed by a large-diaphragm constant pressure stage and penning valve were used to minimize argon flow rate fluctuations; the flow rate was better than ±1 ml min^{-1}. The heating rates were varied from 0.5 to 100° min^{-1}, and the cooling rates were

varied from 0.5 to 50° min⁻¹. Samples were cycled between room tempera-
ture and T_g + 40°C. Not surprisingly, signal resolution was a problem at 0.5,
1 and 2° min⁻¹ heating rates.

The cool/reheat rates of the first run were repeated after the testing
schedule was finished to detect any temperature shifts arising from sample
degradation; there was no detectable shift for any of the samples.

RESULTS

The results are presented in the next three sections. The first section
defines the characteristic temperatures of the glass transition endotherm, and
shows the repeatability of both these parameters, and the heat capacity
change. The second section outlines the method for properly correcting for
the thermal lag at high heating or cooling rates, and the third section shows
the shifts of the characteristic temperatures while varying both the heating
and cooling rates.

Repeatability of endotherm measurements

A typical thermogram displaying the endothermal peak of the glass transi-
tion is shown in Fig. 1. The top schematic defines the typical onset and peak
temperatures. Note that we measure ΔC_p at $T_{\Delta C_p/2}$. The second schematic
of this thermogram denotes the peak area, as typically defined. We also
define the fictive temperature, following the method of Petrie [3], Flynn
[4], and Moynihan et al. [5]; the two areas were matched using a polar
planimeter.

Richardson and Savill [6] determined the fictive temperature by fitting
the liquid and glass heat capacities to quadratic equations (avoiding the
transition region), then determining the intercept temperature of the two. We
attempted a variation of this technique; the enthalpy derivative (mcal sec⁻¹)
was electronically backed off, then fed into an analog integrator. Since the
chart recorder has two pens, the second pen was used to record

$$Y = \int_0^{t'} \left[\left(\frac{\partial H}{\partial t} \right)_p - H_0 \right] dt \qquad (1)$$

Since the heat capacity changes only by 10% at T_g, an electronic back-off
was used to amplify the slope change at T_g; the fictive temperature (the
intercept) was determined visually. Unfortunately, the T^2 term of the inte-
grated heat capacity caused a curved enthalpy line, which limited the
accuracy of intercept determination to ±2°C; the use of a computer interface
would obviously improve repeatability [6].

The bottom trace in Fig. 1 is a thermogram on cooling. Both the onset
temperature and T_x are defined: T_x is the temperature of intersection
between the glass heat capacity line and a straight-line approximation of the
transition region; this intersection was chosen because it is the most repeat-
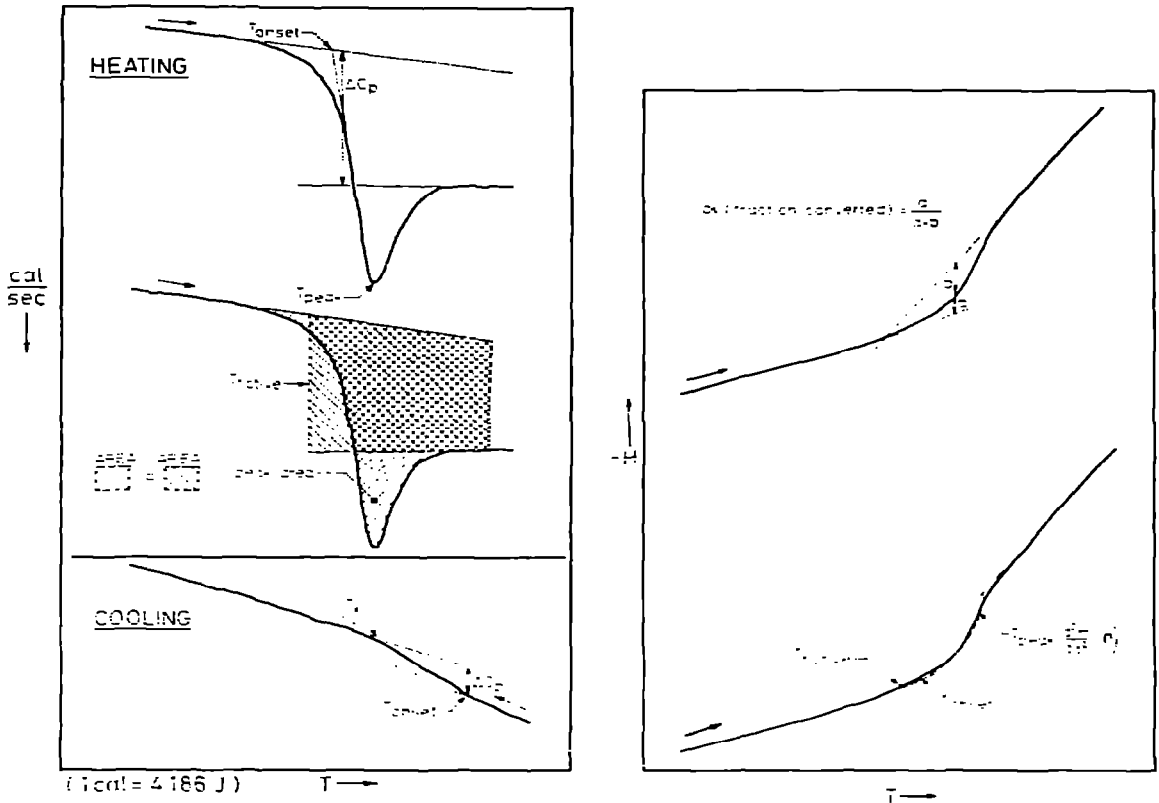able measurement, along with the onset temperature. The heat capacity dif-

Fig. 1. The method of obtaining the characteristic temperatures and peak area from heating and cooling thermograms.

Fig. 2. The redefinition of the characteristic temperatures on an enthalpy—temperature plot. This is the integral of the heating curve in Fig. 1.

ference between the liquid and the glass on cooling is measured at the onset temperature.

The schematics in Fig. 2 are the enthalpy—temperature plots, obtained by integrating the reheating thermograms in Fig. 1. The upper enthalpy trace demonstrates the method of obtaining the fractional conversion (α) at any temperature in the transition range (T_α). In the glass, $d\alpha/dt = 0$, while above the transition region, α is unity. The lower tracing identifies our characteristic temperatures. Since this trace is the integral of the thermograms in Fig. 1, we then see that the peak temperature is now identified as the inflective point in the transition region, whereas before it was the maximum on the thermograms in Fig. 1. The fictive temperature is identified as the extrapolated intersection of the equilibrium liquid and glass enthalpies, in the style of Richardson and Savill [6]. The onset temperature was previously chosen as the intersection of the glass heat capacity line, and a constant slope from the initial peak departure. The integral of this slope is a line of constant curvature, as shown by the dashed segment. The intersection of this curve and the glass equilibrium line is the onset temperature.

Figure 3 is a series of histograms, showing that not all parameter accura-
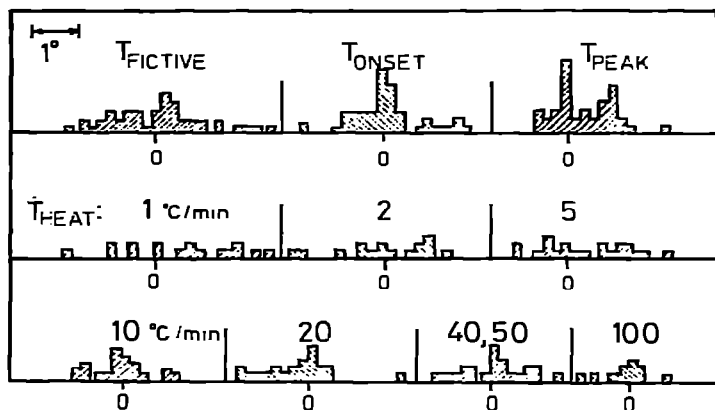
Fig. 3. Histograms of the repeatability of the characteristic temperatures. The first row shows the three temperatures, with results averaged from 5 to $50°$ min^{-1}. The second and third rows show the repeatability of the onset temperature at different heating rates.

cies are equal. The first row shows the distribution of our three characteristic temperatures, averaged over heating rates from 2 to $100°$ min^{-1}.

The standard deviation for the fictive temperature is $±1°C$, about the same as that reported by Richardson and Savill [6]. The onset and peak temperatures are determined with similar repeatabilities, which compare favourably with the standard deviation of $±1.5°C$ for the onset temperature from a recent NBS study [7].

The second and third rows are histograms of the onset temperature at different heating rates. We would expect poorest repeatability at slow heating rates, and this is indeed observed. Once we exceed $5°$ min^{-1}, however, the repeatability remains constant, even at $100°$ min^{-1}. Therefore, tests conducted at high heating rates are quite repeatable. If the instrumental thermal lag arose partially from low sample conductivity, then the transition peak would be broadened, and we would expect poorer repeatability at high heating rates for the extrapolated onset temperature; this is not observed. Since T_{onset} is the extrapolated onset temperature, and not the temperature of initial deviation from the C_p (glass) line, our measuring technique possibly introduces a systematic error at slow heating rates when we try to understand the effects of heat/cool cycles on the onset temperature, but we use this extrapolated temperature because of superior repeatability over the temperature of initial departure [7].

Heat capacity change at the glass transition

The difference in heat capacity between the glass and the liquid has been used to test iso-free volume theories (e.g. Boyer [8]), and to measure hole energies for hole-formation theories [9]. We present our results for $ΔC_p$ in Fig. 4. Note that the four polymers have a $ΔC_p$ which is approximately constant on a per-weight basis, but not on a per-mole basis. The results for PMMA and polysulfone were obtained from runs with a heating rate between
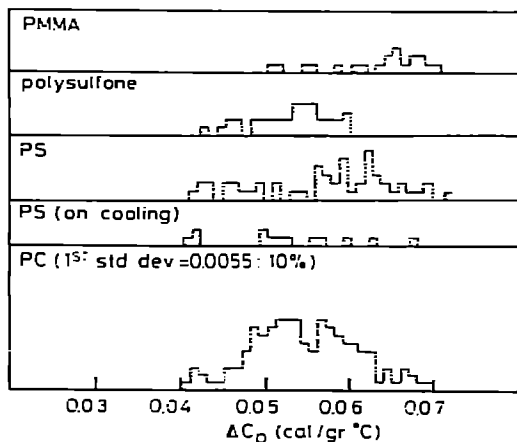
Fig. 4. Histograms of ΔC_p (liquid—glass) at the glass transition for four glassy polymers, showing the repeatability of this measurement.

5 and 50° min^{-1}, and have about equivalent repeatabilities. The PS results contain data from a larger range of heat/cool ratios, but has about the same distribution of ΔC_p as PMMA and polysulfone. The fourth histogram is ΔC_p measured on cooling; we see that the heat capacity change is independent of (PVT) path direction, as expected. The bottom histogram shows a large population of ΔC_p for PC, mainly from annealing results (to be published). Even with the large variation of heat/cool ratios, and the different annealing treatments, the distribution is again ±10%. Goldstein [10] considered the possibility of thermal history effect on ΔC_p, but we found no systematic trend. The heat capacity change could also include effects from anharmonic frequencies in the glass and liquid, but from examination of the Grüneisen constants [11], we will assume that this effect is negligible for polymers near the glass transition at atmospheric pressure.

The value of ΔC_p is easily measured to an accuracy of ±10% (standard deviation). Since ΔC_p is only about 10% of the total heat capacity, we see that the standard deviation is only 1% of the total heat capacity, so this error is reasonable.

TABLE 1

Reported values of $C_{P_{liquid}} - C_{P_{glass}}$ at the glass transition

1 cal = 4.186 Joules.

PS (cal/g°C)	Polysulfone	PC	PMMA
0.061 [a]	0.057 [a]	0.053 [a]	0.065 [a]
0.085 (ref. 12)	0.0705 (ref. 14)	0.0596 (ref. 13)	0.072 (ref. 12)
0.079 (ref. 13)	0.0713 (ref. 16)	0.055 (ref. 18)	0.0817 (ref. 13)
0.0655 (ref. 14)	0.054 (ref.17)	0.060 (ref. 19)	0.074—0.088 (ref. 20)
0.0635 (ref. 15)		0.061—0.079 (ref. 20)	

[a] This work.

However, we might further improve this repeatability by always measuring ΔC_p at the same absolute temperature (e.g. 100°C for PS); we always measured ΔC_p at $T_{\Delta C_p/2}$, and since this temperature is dependent on both the cooling and heating rate, then the non-linear heat capacity variation will force us to measure ΔC_p at different parts of the C_p lines, with resulting different ΔC_p. The solution of using a constant measurement temperature is trivial, but cannot be solely responsible for the large variation in the literature values shown in Table 1 for these four polymers; apparently, large data populations are necessary to obtain accurate ΔC_p values. A heat capacity error of 0.2% would limit ΔC_p determination to ±2% at best.

Thermal lag correction

The thermal lag was measured as a function of heating rate under several different conditions, as shown in Fig. 2. When the DSC cell was first obtained, the thermal lag was measured as a function of heating rate, and it was very small: less than 2° at 100° min⁻¹, for pure indium. This lag was remeasured after a few months in service, after the cell had been operated above 500°C. The constantan disc had visibly oxidized, increasing the instrument— pan lag to 6° at 100° min⁻¹. The increase in sample mass is not responsible for the lag increase, as shown in the Perkin-Elmer DSC II lags: the differ-

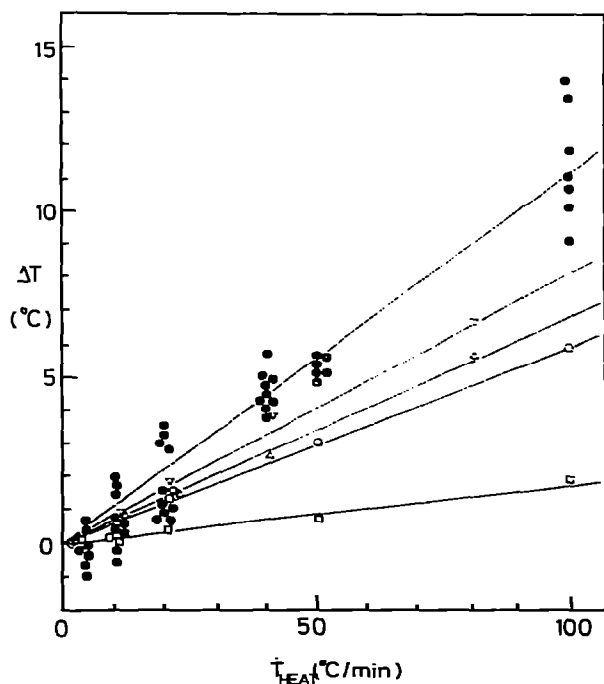

Fig. 5. The linear effect of heating rate on thermal lag in a DSC instrument. △, Indium (3 mg), tested in a Perkin-Elmer DSC II; ▽, benzoic acid (13 mg), tested in a Perkin-Elmer DSC II; ○, indium (14 mg), tested in a DuPont 990; ◇, indium, results reported by Barton [21] with a DuPont 990; □, indium (4 mg), tested in a new DuPont 990; ●, anionic polystyrene (3 mg), tested in a DuPont 990 (points are the fictive temperature).
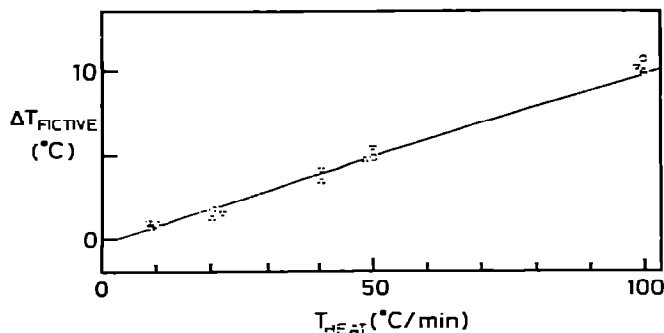
258

Fig. 6. The thermal lag for polystyrene (○), polysulfone (△), and polycarbonate (▽); each point is the average of several runs of the fictive temperature lag.

ence in thermal lag between 3 mg indium and 13 mg benzoic acid measures the additive effects of superheating, thermal conductivity and sample mass: the difference between indium and benzoic acid was small, relative to the lag due to pan—instrument resistance. The thermal lag for the oxidized disc matches the lag reported by Barton, who also used a DuPont 990 [21]. The solid circles in Fig. 5 are the fictive temperature for anionic polystyrene: these points were shifted with the lag at +5° min^{-1} arbitrarily set to zero for each cooling rate.

The fictive temperature should be independent of the heating rate [3,15], so the observed shift due to heating rate is the thermal lag, which includes lags due to instrument—pan resistance, sample—pan resistance, and sample conductivity. The fictive temperature shift (equal to the thermal lag) is plotted as a function of heating rate for polystyrene (PS), polycarbonate, and polysulfone in Fig. 6. Each point is the average of between 2 and 10 runs. Since all three polymers have nearly the same heat capacity, thermal conductivity and surface emissivity, we would expect the thermal lag to be the same for all three polymers. This equivalence in Fig. 6 supports the assumption that the fictive temperature is path-independent.

Characteristic temperature shifts

Fictive temperature
We have forced the fictive temperature to be independent of the heating rate, thus calibrating the instrument thermal lag. Figures 7 and 8 show the (corrected) fictive temperature as a function of cooling rate; the shift of the fictive temperature per decade (cooling rate) is 2.2°C for PS, and 2.9°C for polysulfone. Note, however, that the fictive temperature asymptotically approaches a limiting value at fast cooling rates. This trend is apparent for both polystyrene and polysulfone; previous results reported a linear shift over the entire experimental (log) cooling rates, but the cooling rates were slower than the rates used in this study, which are more typical of the cooling rates used in industry.
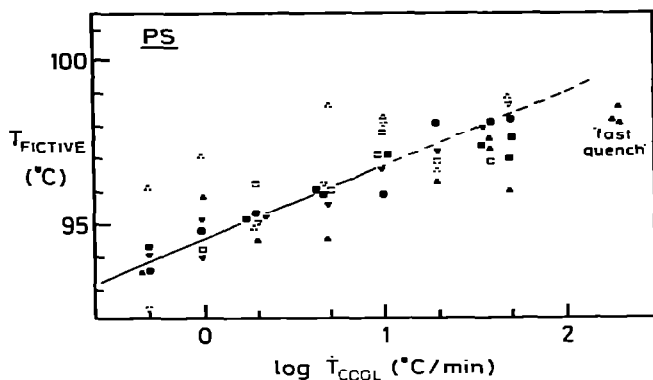
Fig. 7. The effect of cooling rate on the fictive temperature for polystyrene. Results at different heating rates have been corrected for thermal lag, using results from Fig. 6. Heating rate (°C min⁻¹): △, 1; ▽, 2; □, 5; ●, 10; ▲, 20; ▼, 40; ■, 50.

Onset and peak temperatures

The onset and peak temperatures, even when corrected for thermal lag, still vary with the heating rate. Figure 9 shows both (corrected) temperatures for polystyrene, plotted against the log heating rate; both temperatures shift linearly with the log heating rate. The peak temperature is approximately independent of cooling rate for PS. Before we proceed further, Fig. 9 is significant, so we should state the important trends exhibited in this graph.

(1) The onset temperature decreases with increasing cooling rate. The onset temperature reaches a minimum value (97°C for PS, 183°C for polysulfone) when the heating rate is equal to, or less than the cooling rate.

(2) For PS and polysulfone, the limiting onset temperature (on reheating) is higher than T_x, measured while cooling.

(3) The onset and peak temperatures shift at the same rate when the heating rate is increased: since their slopes are always the same, these two temperatures can be considered as characteristic temperatures of the endotherm,
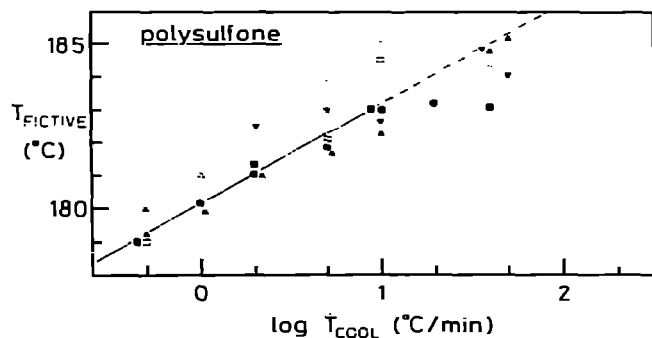

Fig. 8. The effect of cooling rate on the fictive temperature for polysulfone. Results at different heating rates have been corrected for thermal lag, using results from Fig. 6. Heating rate (°C min⁻¹): △, 1; □, 5; ●, 10; ▲, 20; ▼, 40; ■, 50.
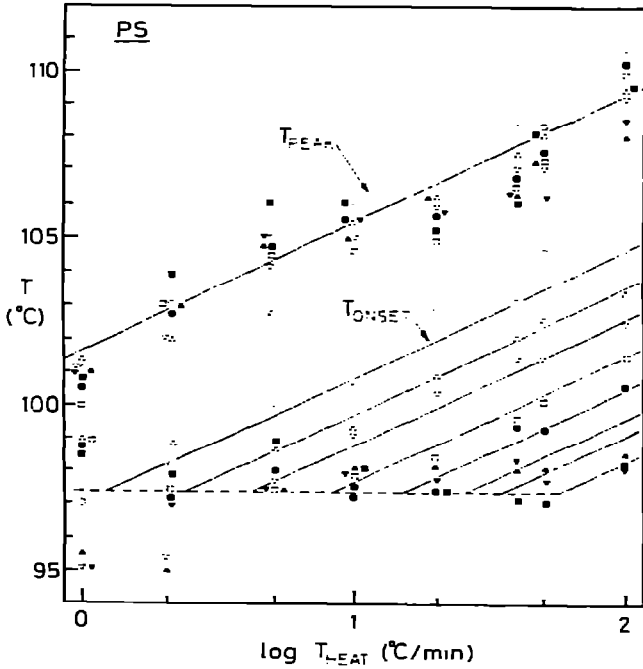
Fig. 9. The corrected peak and onset temperatures (on reheating) plotted against (log) heating rate for polystyrene. Lines are constant cooling rate. Cooling rate (°C min⁻¹): ○, 0.5; △, 1; ▽, 2; □, 5; ●, 10; ▲, 20; ▼, 40; ■, 50.
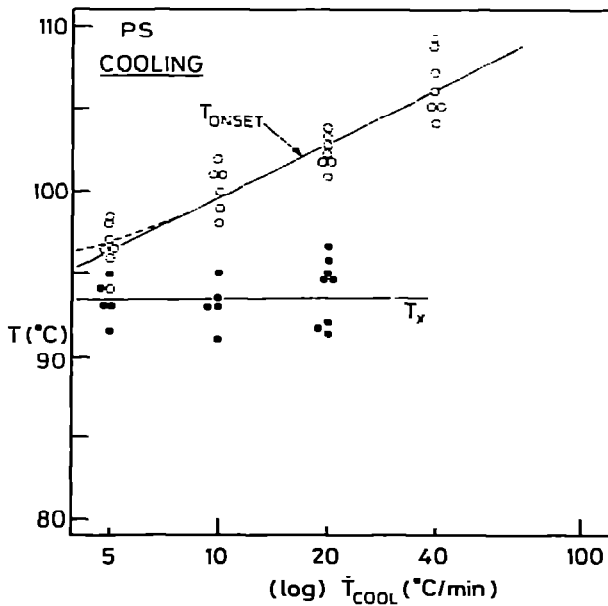

Fig. 10. The corrected onset and "cross' temperatures for polystyrene, measured while cooling.
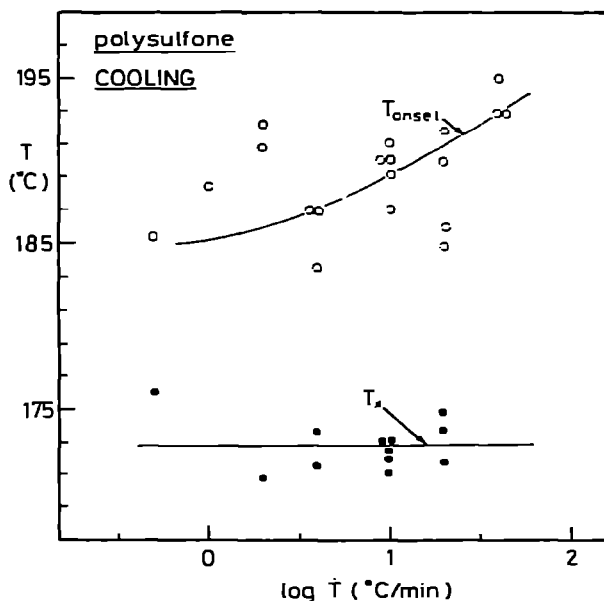
Fig. 11. The corrected onset and "cross" temperatures for polysulfone, measured while cooling.

and can be used to characterize transition behavior.

(4) The onset temperature shift due to a heating rate increase is the same as the shift due to a cooling rate decrease, suggesting that the heat/cool ratio may be the significant experimental parameter for controlling enthalpy relaxation on reheating.

The onset and extrapolated "cross" temperatures were obtained from a limited number of cooling thermograms only for polystyrene and polysulfone; results are shown in Figs. 10 and 11. The onset temperature shifts with cooling rate much faster than any previously-determined temperature shift. The slope of this line yields an apparent activation enthalpy of 85 kcal mole^{-1} (measured at the high temperatures) for polystyrene, compared to viscosity measurements of 82 kcal mole^{-1} [22].

DISCUSSION

Experimental technique

This work used a "DSC type" instrument, but since the heat flow at the glass transition is less than 10 mcal sec^{-1} (using a 10 mg sample), the difference between DSC and DTA machines is negligible.

The resolution of a thermal analyzer is limited by the RMS noise level of the ΔT amplifier, which with current instrumentation amplifiers is about 1 μV. This noise level should be compared with the generated e.m.f. from a thermoelectric junction: between 20 and 50 μV $^{\circ}$C^{-1}, limiting machine resolution to a ΔT of about 0.02°C. This limitation can be translated into mcal if the cell heat capacity is known.

The repeatability of a thermogram depends on sample mass and geometry, pan placement, and gas flow fluctuations. This problem of gas flow variation between the sample and reference cells prevented the measurement of the glass transition on cooling with a Perkin-Elmer DSC-II instrument.

Correcting for thermal lag

The one basic assumption in this paper is that by artificially reconstructing the T_g endotherm into an instantaneous "ideal" glass transition, heating rate effects are eliminated (Fig. 1). This is equivalent to assuming that the enthalpy required on reheating to bring a glass back to an (equilibrium) liquid is path-independent. When we plot the fictive temperature as a function of heating rate, we are actually calibrating for the total instrumental lag, including lags due to instrument—sample resistance, sample—pan resistance, and low sample thermal conductivity. This self-calibration is the best way to calibrate for machine lag in glassy polymers. A bulk sample can be tested, regardless of its size (within reason), then quenched at a controlled rate and reheated. The fictive temperature upon reheating can then be compared with the expected fictive temperature at that cooling rate, and the resulting temperature difference is the instrumental lag for that specific sample. This measured thermal lag is quite reasonable (Fig. 5) and we also see that if the indium lag was used alone we would be seriously in error at high heating rates. Note, also, that the lag is a linear function of heating rate, with the additional lag above that of indium arising from the pan—sample resistance. The lag is not due to low thermal conductivity, or the lag would be non-linear with heating rate. This is reassuring, as the sample mass (~ 3 mg) is less than the critical mass (>8 mg) at which the low thermal conductivity should start to cause peak distortion.

Characteristic temperature shifts

The shift of the fictive temperature with cooling rate was measured for all four polymers, and compared with the α peak shift, measured dielectrically at 100 Hz. These results are shown in Table 2. Although it has been suggested that these two should be the same [5], there is no correlation. Also, the fictive temperature "apparent activation energy" is nearly constant for all four polymers, even though this apparent activation energy should

TABLE 2

Comparison of activation energies from dielectric and fictive temperature methods

	E_a (dielectric) [a] (kcal mole^{-1})	ΔH_a ($T_{fictive}$) (kcal mole^{-1})	T_g (°C)
PS	120	270	95
PMMA	60	300	110
Polycarbonate	150	240	150
Polysulfone	180	260	185

[a] Ref. 8.

increase with increasing glass transition temperature [8].

The shifts of the onset and peak temperatures are important in three ways. (1) Both characteristic temperatures display the same slope, which is linear with (log) heating rate. This slope is not the same as the slope for the fictive temperature shift. (2) The onset temperature reaches a limiting minimum value when the heating rate equals the cooling rate. (3) The onset temperature is constant when replotted at constant cool/reheat ratio. These three conclusions, along with peak area and peak shape results will be discussed in future papers from this DSC study.

Measurements during cooling

For PS, the extrapolated "cross" temperature is apparently constant at about 93°C; this is about 5° less than the limiting onset temperature measured from glass reheating experiments. We see that the apparent activation energy rapidly increases as the glass transition region is approached. Extrapolation below 5° min^{-1} cooling rates would result in a crossing of the two lines, which is impossible. Therefore, a curved line is drawn for either the onset temperature or T_x at slow cooling rates; unfortunately we could not reproducibly measure the enthalpy change at the slow cooling rates. Comparing the results for polysulfone with those for PS, we see that T_x is again constant, and the onset temperature shifts in the same way as for PS. Note the temperature difference between the onset and "cross" temperatures. This is the transition region on cooling, and is a much larger temperature span for polysulfone than for PS. We can mathematically express this, via the WLF equation, by saying that $(T_g - T_0)$ is larger for polysulfone than for PS.

We can empirically reshape the cooling curve to determine T_f while cooling (Fig. 1). From the simple shape of the C_p change on cooling, we expect $T_f \approx (T_{on} + T_x)/2$. As expected from the simple reconstruction, we see that T_f (Figs. 8 and 9) falls about half-way between T_{on} and T_x on cooling (Figs. 10 and 11). Therefore, according to this qualitative reconstruction, the fictive temperature is the same value, whether measured while cooling or reheating; the fictive temperature is path-independent.

CONCLUSIONS

(1) When the flushing gas is properly regulated, and the sample—pan interface is maintained, then the glass transition can be measured during both cooling and reheating with sample masses as low as 2 mg.

(2) If the sample mass is less than about 8 mg, then the thermal lag at high heating rates arises mainly from the combined instrument—pan and sample—pan interfaces. The path-independency of the fictive temperature (equivalent to the excess enthalpy) can be exploited to correct for the thermal lag in glassy polymers, even when large samples (i.e. mass >8 mg) are studied.

(3) The variation of the fictive temperature with cooling rate does not correspond with viscosity or dielectric results. The fictive temperature asymptotically approaches a limiting value at fast cooling rates (at atmospheric pressure).

(4) The onset temperature (on reheating) reaches a minimum value as the reheating rate becomes slower than the cooling rate.

(5) The shift of the onset temperature, measured while cooling, is consistent with viscosity and dielectric results for polystyrene. Although the results are less accurate for polysulfone, this same conclusion is also apparently true for polysulfone.

ACKNOWLEDGEMENTS

REFERENCES

1   E. Pella and M. Nebuloni, J. Therm. Anal., 3 (1971) 229.
2   J.K. Gillham and R.F. Boyer, J. Macromol. Sci. Phys., 3 (1977) 497.
3   S.E.B. Petrie, J. Polym. Sci. Part A-2, 10 (1972) 1255.
4   J.H. Flynn, Thermochim. Acta, 8 (1974) 69.
5   M.A. DeBolt, A.J. Easteal, P.B. Macedo and C.T. Moynihan, J. Am. Ceram. Soc., 1—2 (1976) 16.
6   M.J. Richardson and N.G. Savill, Polymer, 16 (1975) 753.
7   P.D. Garn and O.J. Menis, J. Macromol. Sci. Phys., 4 (1977) 611.
8   R.F. Boyer, J. Macromol. Sci. Phys., 3 (1973) 487.
9   B. Wunderlich, J. Therm. Anal., 5 (1973) 117.
10 M. Goldstein, J. Chem. Phys., 11 (1976) 4767.
11 F.I. Mopstik and M.G. Broadhurst, J. Appl. Phys., 10 (1973) 4261.
12 V. Bares and B. Wunderlich, J. Polym. Sci. Phys., 11 (1973) 1301.
13 B. Wunderlich, J. Chem. Phys., 37 (1962) 2429.
14 G. Kanig, Kolloid Z. Z. Polym., 233 (1969) 54.
15 R.J. Roe, Bull. Am. Phys. Soc., 22 (1977) 429.
16 W.J. Wrasildo, Adv. Polym. Sci., 13 (1974).
17 P. Zoller, J. Polym. Sci., Polym. Phys. Ed., 16 (1978) 1261.
18 N. Van Bach and C. Noel, J. Polym. Sci. Part A-1, 14 (1976) 1627.
19 J.H. Flynn and L.A. Wall, J. Res. Natl. Bur. Stand. Sect. A, 70 (1968) 478.
20 J.J. Gedemer, Plast. Eng., 20 (1975) 249.
21 J.M. Barton, Thermochim. Acta, 20 (1977) 249.
22 J.N. Hay, Polymer, 19 (1978) 1224.